Journal of Materials Chemistry A

ROYAL SOCIETY OF CHEMISTRY

PAPER

View Article Online
View Journal | View Issue

Cite this: J. Mater. Chem. A, 2025, 13, 12625

Solvometallurgy: design of ternary deep eutectic solvents for the electrochemical recovery of nickel from lithium-ion cathode materials†

Suchithra Ashoka Sahadevan, [a] Mohamed Shahid, [b] Shrihari Sankarasubramanian [bc] and Vijay Ramani *[a]

Recovering critical metals from lithium-ion batteries (LIBs) is crucial for resource conservation and waste management. Current LIB recycling methods, such as pyrometallurgy and hydrometallurgy, have limitations in the selective recovery of pure metals, waste management, *etc.* Deep Eutectic Solvents (DESs) show potential for recycling critical metals from the cathode materials due to their non-toxic components and low cost. However, they are often limited by high leaching temperatures (140–220 °C) and insufficient recovery methods for leachate solutions. Here, we present the design of a ternary DES (T-DES) of choline chloride (ChCl), ethylene glycol (EG), and citric acid (CA), optimized for both metal leaching and electrochemical recovery. This T-DES achieved high leaching efficiencies (LEs) of 99 ± 2% and 98 ± 4% for Li and Ni at 70 °C. Nickel was successfully recovered from the leachate using electrodeposition, with performance enhanced by optimizing the substrate material, temperature, time, and viscosity. Notably, viscosity reduction, achieved by modifying T-DES molar components, improved faradaic efficiency (FE) by up to 65% (−0.8 V *vs.* Ag). The T-DES achieved high LE for the NMC cathode material, with 94 ± 8% for Li, 99 ± 6% for Mn, 85 ± 6% for Ni, and 99 ± 3% for Co at 90 °C, demonstrating broader applicability to other LIB cathode materials. Scanning electron microscopy-energy dispersive X-ray spectroscopy validation revealed pure metal deposition. Additionally, our findings indicate that the T-DES design is promising for efficient and environmentally friendly metal recovery from LIB waste, advancing sustainable battery recycling technologies.

Received 29th November 2024
Accepted 13th March 2025

DOI: 10.1039/d4ta08483g

rsc.li/materials-a

1 Introduction

The increasing use of lithium-ion batteries (LIBs) in vehicles and energy storage systems has consequently increased LIB waste.[1–3] Spent LIB cathode material typically consists of critical metals such as cobalt (Co) (5–10 wt%), nickel (Ni) (5–10 wt%), manganese (Mn) (10–15 wt%), and lithium (Li) (5–8 wt%) which are in high demand and of limited production.[2,3] Hence, recycling metals from LIBs has become a significant topic of interest, as it addresses the environmental concerns associated with landfilling LIB waste and promotes resource conservation by reducing the need for mining.[4–6]

Current LIB recycling methods include pyrometallurgy and hydrometallurgy.[6] Pyrometallurgy involves high temperatures to recover metals, which often causes the evolution of hazardous gases, high energy consumption, and low efficiency. Hydrometallurgy involves leaching metals from the black mass (spent LIBs subjected to physical size reduction) using acids such as sulfuric acid (H_2SO_4) with reducing agents such as hydrogen peroxide (H_2O_2). Metals are recovered from the leachate solution using different separation methods, precipitation, and adsorption, depending on the desired metal recovery.[7,8] However, each method has limitations in yielding selective metal recovery, high energy consumption, waste management, *etc.*[9–11] Hence, we are searching for new and inexpensive technology to effectively recover metals with low energy consumption, high selectivity, and the least environmental concerns.

Solvometallurgy is an alternative method of LIB recycling that utilizes a non-aqueous solvent. Deep Eutectic Solvents (DESs) have received significant attention in LIB recycling for their metal leaching efficiency and eco-friendliness.[12–16] DESs are eutectic mixtures made of a hydrogen bond acceptor (HBA), typically choline chloride (ChCl)) and a hydrogen bond donor (HBD), such as ethylene glycol (EG), urea, *etc.*[17–20] Tran *et al.* pioneered using a 1:2 ChCl:EG (12 CE) DES for leaching Li and Co metals from lithium cobalt oxide (LCO) at 180 °C for 24 h and achieved a leaching efficiency (LE) of 94% and 89%,

[a]Department of Energy, Environmental, and Chemical Engineering, Washington University in St. Louis, 1 Brookings Drive, Missouri, 63130, USA. E-mail: ramani@wustl.edu

[b]Department of Biomedical Engineering and Chemical Engineering, University of Texas at San Antonio, San Antonio, TX 78249, USA

[c]Department of Mechanical, Aerospace and Industrial Engineering, University of Texas at San Antonio, San Antonio, TX 78249, USA

† Electronic supplementary information (ESI) available. See DOI: https://doi.org/10.1039/d4ta08483g

respectively.[21] Subsequently, Co was precipitated as a mixture of carbonate and hydroxide byproducts.

Various DESs such as ChCl:urea and ChCl:organic acid combinations (citric acid (CA), tartaric acid, *etc.*) have been investigated for leaching metals from LCO and lithium nickel manganese cobalt oxide (NMC) cathode materials.[22,23] The reducibility nature of HBD components, such as EG and urea, plays a vital role in reducing the transition metals Co/Ni/Mn to their lower oxidation state and contributes to leaching.[24,25] Incorporating carboxylic acid as an HBD component significantly increases the leaching ability in reduced time. However, the high viscosity (*e.g.*, ChCl:tartaric acid-6840 mPa s) of most organic acid-based DESs limits their potential for future applications.[26,27] Metal recovery from leachate solutions remains an area with limited research. Kerstin *et al.* reported using a ChCl:tartaric acid DES to leach metals from NMC and further regenerate NMC from the leachate solution using the anti-solvent crystallization method.[12]

DESs also possess a wide range of electrochemical stability windows (ESWs). For instance, 12 CE demonstrates a good ESW (3.15 V *vs.* Ag wire), with a cathodic onset potential at −1.8 V *vs.* Ag wire and an anodic onset potential at 1.35 V, enabling electrodeposition.[15,28] Electrodeposition shows promise for selectively recovering metals with high purity and minimal environmental impact compared to other separation methods. Few studies have demonstrated the recovery of Co from LCO using different DESs.[15,29] However, limited studies have been conducted on the electrochemical recovery of other metals, such as Ni and Mn, from leachate solutions using DESs.[20] Lithium nickel oxide (LNO) is a key cathode material that has gained renewed interest in high-energy-density applications, such as high-voltage lithium-ion batteries, which offer higher capacity and lower cost than LCO.[30,31]

This work proposes the design of a new T-DES that fulfills the requirements for efficient leaching and electrodeposition. We synthesized a T-DES composed of ChCl, EG, and CA in a 1 : 2 : 1 molar ratio, demonstrating synergistic improvements in viscosity, overall leaching efficiency, and electrochemical stability. The Ni species in leachate solutions are further investigated using UV-visible spectroscopy to understand the metal speciation. Electrochemical studies of the T-DES and the leachate solution are conducted, and Ni from the leachate solution is electrodeposited on substrates such as copper sheets and carbon paper. The effects of applied potential, substrate stability, temperature, and time are studied. This study represents the first investigation of the electrochemical recovery of Ni from the LNO cathode material using a DES. The following acronyms are used in this work: 1:2 ChCl:EG – 12 CE; 1:1 ChCl:CA – 11 CC; 1:2:1 ChCl:EG:CA – 121 CEC.

2 Results and discussion

2.1 Design and characterization of the ternary DES

TDES systems represent an emerging approach for tailoring physicochemical properties, building on the extensive exploration of the binary DES (B-DES). Recent examples of TDESs for LIB recycling include citric acid : choline chloride : ethylene glycol (1 : 1 : 1), maleic acid : guanidine : ethylene glycol (1 : 1 : 2), and glycine : ascorbic acid : water (1 : 1 : 30).[32–34] These systems have been used for leaching, metal precipitation, and LCO resynthesis, leveraging their acidity and reducing ability, coordination capacity, and viscosity.

Carboxylic acids, such as maleic and citric acid, were selected for their high proton activity and ability to form carboxylate complexes, enhancing the dissolution of metal oxides. EG acts as a reducing agent, while water reduces viscosity. C. Ferrara *et al.* identified 1 : 1 : 1 ChCl : EG : CA as a TDES with a balance of acidity, reducing ability, and viscosity.[34] Glycine: ascorbic acid: water was recognized for its acidity, coordination capability, and reducing properties.[32] However, electrochemical stability becomes critical for TDESs designed for electrochemical recovery, as water often reduces stability due to hydrogen oxidation and reduction (Fig. S1†).

In this study, to obtain the desirable LE of Li and Ni from LNO and to recover Ni metal by electrodeposition, three critical parameters were considered: (i) minimizing transport limitations by maintaining a viscosity of ≤2500 mPa s at room temperature (RT), (ii) utilizing reducing agents and acidic HBDs in the DES components to leach metals from cathode materials (leaching ability >90%), and (iii) ensuring electrochemical stability at negative potential (∼−1.4 V *vs.* Ag wire) for Ni reduction. ChCl is a commonly used HBA because of its wide availability, low toxicity, and biodegradability. ChCl:urea is the first reported DES for leaching studies. Since then, various HBD (amines, alcohols, carboxylic acids) have been combined with ChCl to form stable DESs.[19,23,35] 12 CE is a popular DES used for leaching metals and electrolytes for electrodeposition due to its reducing nature to dissolve metal oxides, low viscosity (37 mPa s), and wide ESW under ambient conditions (3.15 V *vs.* Ag wire).[19,23,35] Despite these advantages, EG requires harsh conditions to leach high-valent metal oxides.[36,37] Carboxylic acids exhibit higher leaching ability due to their high proton activity and ability to form carboxylate complexes with metal ions, enhancing the solubility of metal oxides by reacting with the oxygen atoms in metal oxides and cleaving the metal–oxygen bonds (eqn (1)–(3)).[25,36,38]

$$\mathrm{H{-}L} \leftrightarrow \mathrm{H_{DES}}^{+} + \mathrm{L_{DES}}^{n-} \quad (1)$$

$$\mathrm{M{-}O} + \mathrm{H_{DES}}^{+} \leftrightarrow \mathrm{M{-}O\cdots H}^{+} \quad (2)$$

$$\mathrm{M{-}OH}^{+} + \mathrm{H_{DES}}^{+} + \mathrm{L_{DES}}^{n-} \leftrightarrow \mathrm{M{-}L_{DES}}^{n-1} + \mathrm{H_2O} \quad (3)$$

CA, a triprotic acid (pK_a ∼3.13, 4.76, and 6.4), is widely used in hydrometallurgy as a renewable, non-toxic, and abundant mild reducing agent for leaching (Table S1†).[39] The hydroxyl and carboxylate ions of CA may coordinate with metals and facilitate leaching.[40–42] However, carboxylic acid-based DESs, such as ChCl:CA, led to highly viscous DESs (1 : 1 – 9126 mPa s), limiting their practical applications. To address this, we designed a T-DES composed of 121 CEC to improve LE, ESW, and viscosity. Different molar compositions (molar ratios of 1 or 2) of ChCl : EG : CA were initially tested, and the composition with the least viscosity and forming uniform liquid at RT was chosen for

further studies (Fig. S2†). Consequently, 121 CEC was selected. In the CA-based DES (121 CEC), leaching occurs *via* Ni^{3+} reduction to Ni^{2+}, formation of metal chloride complexes, and proton reactions with oxide species to produce water. The synergy between EG enhances mass transportation by reducing viscosity; CA (H^+ provider and coordination) and ChCl (chloride ligands) aid in metal dissolution.[22]

T-DESs are characterized using Fourier-transform infrared spectroscopy (FT-IR) (Fig. S2†), viscosity and conductivity measurements (Fig. S3†), and thermogravimetric analysis (TGA) (Fig. S4†). FT-IR analysis confirmed the formation of 121 CEC, as indicated by the characteristic peaks of functional groups from corresponding precursors and hydrogen bonding interactions between them (Fig. S2b†). A detailed discussion of peak assignment is provided in the ESI.†[39,43,44]

The viscosity and conductivity of 121 CEC as a function of temperature are shown in Fig. S3.† The viscosity values were found to cover the range of 50 to 2500 mPas for varied temperatures (290–360 K). As expected, the viscosity decreased with temperature while the conductivity increased. For instance, viscosity is reduced by more than 12 times from 2400 mPa s at 298 K to 190 mPa s at 358 K (Fig. S3†), whereas the conductivity increased from 0.3 mS cm^{-1} at 298 K to 5.5 mS cm^{-1} at 358 K. The temperature-dependent conductivity obeys the Arrhenius equation and shows a good linear fit (Fig. S3†). The activation energy was calculated from the relation and was found to be 52 kJ mol^{-1}.

The thermal stability of 121 CEC and the precursors were measured using TGA, as shown in Fig. S4.† There are three decomposition steps for 121 CEC (blue dotted line). Initially, there is a slight decrease in weight (<10%) between 373 and 393 K, which could be from the evaporation of absorbed water molecules during the sample preparation as ChCl is highly hygroscopic and due to degradation of EG, as evidenced from the weight loss of EG (green line). A significant decomposition happens in the second step, 430–465 K; this could be attributed to the degradation of CA, as the CA starts to degrade around 450 K (pink line). At high temperatures, >473 K, the degradation of ChCl happens (black line). Water uptake affects viscosity, complexation, and electrochemical stability. The DES was handled and stored under dry conditions to mitigate these effects.

2.2 Leaching

For the leaching studies, 0.1 g of LNO was dissolved in 5 g of 12 CE and 121 CEC at 363 K for 24 h. As the leaching proceeded using 121 CEC, the color of the DES progressively shifted from black to dark green, whereas 12 CE did not exhibit any color change under the same conditions (Fig. 1a and d). The color of the leachate solution also directly indicates the leaching of ions from oxide into solutions, which is confirmed by the ICP-OES analysis (Fig. 1a–f). The LE of Li and Ni in 12 CE is 19 ± 2% and 3 ± 1%, respectively, whereas, with 121 CEC, LE is significantly increased to 100 ± 5% and 98 ± 2%, respectively. The difference in LE of metals in 12 CE and 121 CEC can be attributed to the complementary roles of CA and EG.[22] Although EG is a strong reducing agent, previous literature and experimental results evidence that this process requires harsh leaching conditions (T > 140 °C).[36,37] CA, with pK_a values of ~3.13, 4.76, and 6.4, is a moderately strong acid that readily donates protons under mild conditions. Upon deprotonation, the carboxylate groups of the citrate ion coordinate with metal ions, forming stable complexes that enhance solubility. In contrast, EG has weaker complexing abilities (pK_a ~15) and a neutral pH (~7) than CA.[25,36,38] The presence of EG in the 121 CEC T-DES mitigates the high viscosity, promoting mass transfer. To optimize the

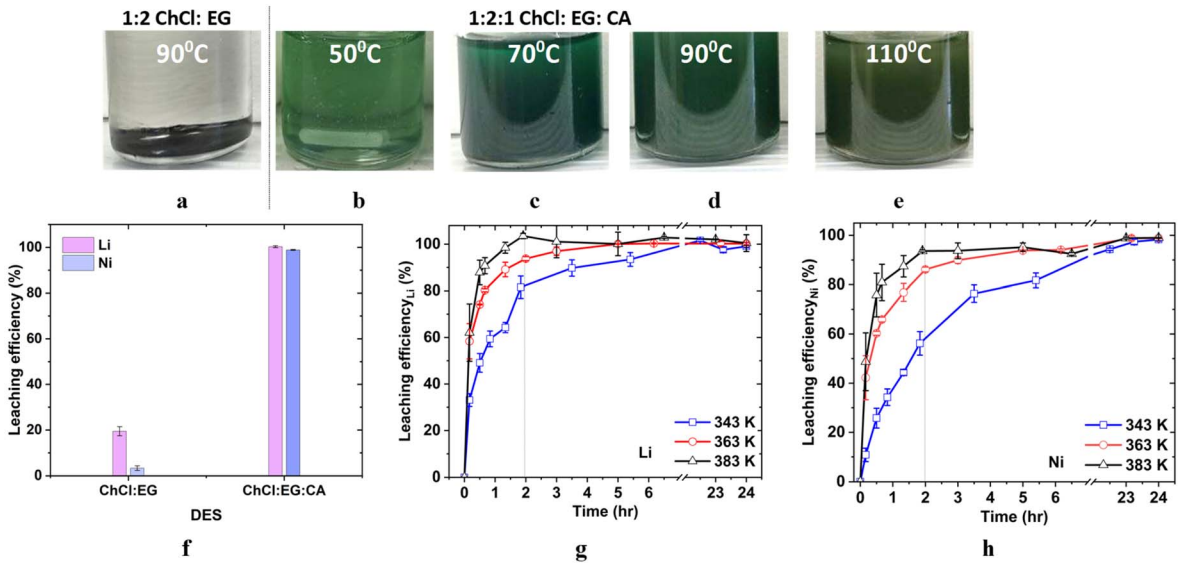

Fig. 1 Photograph of the leachate solution in different DESs and temperatures after 24 h: (a) 12 CE leachate solution at 363 K; (b–e) 121 CEC leachate solution at varied temperatures 323–383 K from left to right, respectively; (f) comparison of LE of Li and Ni metals using 12 CE and 121 CEC DES under the same leaching conditions(363 K, 24 h); (g) LE of Li at different temperatures over time; (h) LE of Ni at different temperatures over time. The error bars represent standard errors calculated from three independent experiments.

leaching temperature for the T-DES, leaching was performed at different temperatures (323, 343, 363, and 383 K) for 24 h (Fig. S5†). LE of Li and Ni increased with temperature. For 323 K, the LE of Li and Ni was 49 ± 6% and 13 ± 4%, respectively. For a temperature >343 K, the LE of both Li and Ni drastically increased to >95%.

The optimization of leaching time (0–24 h) for Li and Ni was performed at temperatures ranging from 343–383 K (Fig. 1g–h). It was observed that significant leaching of metals occurs during the initial period (t < 2 h) at all temperatures. For example, at 363 K, Li reached approximately 94% LE within 2 h, while Ni required 5 h to achieve the same LE. At 383 K, Li reached 100 ± 3% LE within 2 h, whereas 93 ± 0.6% LE was obtained for Ni.

2.2.1 Speciation of Ni in leachate solutions: UV-VIS spectroscopy. UV-VIS spectroscopy was performed to analyze the Ni species in 12 CE and leachate solutions with 121 CEC at 323 K and 358 K (initial electrodeposition conditions). For 12 CE, $NiCl_2 \cdot 6H_2O$ was used instead of leachate, as Ni levels in the leachate were below detection limits. At RT, the 12 CE spectra showed two absorption bands centered at 420 nm (band I) and 694–761 nm (band II), corresponding to $[NiCl_3(EG)_3]^{2-}$and $NiCl_4^{2-}$, respectively. These bands indicate the electronic transition of $^3A_{2g}(F) \rightarrow {}^3T_{1g}(P)$ for octahedral and $^3T_1(F) \rightarrow {}^3T_1(P)$ for tetrahedral complexes (Fig. S7a,† blue line).[45,46]

In contrast, the 121 CEC leachate exhibited a blue shift to 404 nm and 690–747 nm at room temperature, suggesting significant changes in the Ni coordination environment due to interactions with CA or chloride ions, possibly forming complexes such as $[NiCl_x(Sov)_y]^{2+}$ (where Sov denotes solvent or ligand donor species), as supported by previous literature (Fig. S7b,† blue line).[44,47,48]

Moreover, Ni complexes in DESs and ionic liquids often exhibit reversible thermochromism at elevated temperatures.[45,46,49] For 12 CE, at 358 K, band II intensity increased due to the conversion from octahedral to tetrahedral configuration (eqn (4)) (Fig. S7a,† green line). This was attributed to the solvolysis of EG on Ni^{2+}.[45]

$$[NiCl_3(EG)_3]^- + ChCl_2^- \text{ (Octahedral, low temp)} \leftrightarrow [NiCl_4]^{2-} + 3EG \text{ (Tetrahedral, high temp)} \quad (4)$$

However, in 121 CEC, the spectra remained unchanged at 358 K, indicating a stable Ni coordination environment dominated by CA and chloride interactions (Fig. S7b,† green line). The absence of thermochromism within this temperature range (323–358 K) suggests that the introduction of CA stabilizes the octahedral coordination structure, preventing the transition to a tetrahedral geometry. A similar lack of thermochromism was observed with the ChCl:urea DES, attributed to differences in metal speciation compared to 12 CE.[45] This further supports the distinct coordination environments and speciation in 12 CE and 121 CEC.

2.2.2 Leaching kinetics. Leaching kinetics were analyzed using shrinking core models (SCMs), mixed control reactions, and the Avrami model (eqn (11–15), ESI†) to understand the leaching mechanism.[50,51] Among these models, the SCM aligns with the experimental data (Tables S2 and S3†) and forms the basis for the proposed leaching mechanism shown in Fig. 2a.[26,52] Leaching with 121 CEC achieved high LE, highlighting CA's role in facilitating the process. In the kinetics framework, proton interactions from CA initiate the breakdown of the cathode material, enabling subsequent reactions. The main three steps in the SCM are: (i) interaction with the leaching agent (in this case, CA, EG, H^+, *etc.*) at the surface of the cathode material (liquid boundary layer mass transfer reaction, eqn (11), ESI†) (ii) chemical reaction between the leaching agent and reaction core, forming the product (surface chemical reaction, eqn (12), ESI†) (iii) diffusion of the Ni^{2+}-CA-EG and LiCl complexes into the DES through the solid product layer (residue layer diffusion reaction, eqn (13), ESI†).[27,53,54]

As 100% LE is obtained for Li at 383 K in 120 min, all the kinetics studies are performed in the time range of 0–120 min and at temperatures of 343–383 K. The data were fitted to all the steps (eqn (11)–(15)†) to analyze the kinetics. The fitting with eqn (11)† was poor (R^2 < 0.7); hence, it was neglected. The R^2 and rate constant for eqn (12)–(15) are shown in Table S2 and S3.† From the linear fitting of a straight line, it is observed that equation 13 exhibited a good R^2 of fitted lines for all temperatures (R^2 > 0.93), indicating that diffusion is the rate-determining step for both Li and Ni (Fig. 2b and c). The rate constant k is calculated from the slope of the linear fit. From the plot of $\ln K$ *vs.* $(1/T)$ for each temperature, the activation energies were calculated to be 25 and 38 kJ mol^{-1} for Li and Ni, respectively (Fig. S6†). These E_a values are comparable with other systems exhibiting diffusion-controlled leaching processes (Fig. 2a). The slower leaching of transition metals compared to Li is also observed in other cathode materials, such as LCO and NMC. In LNO, Li^+ is intercalated into the layered nickel oxide (Fig. 2a right).[55] Li^+ quickly emerges upon interaction with acid, whereas Ni^{3+} has to undergo a redox reaction and form Ni^{2+} complexes to dissolve in the leachate, for which higher activation energy is required.[22,53,56]

2.3 Electrochemical studies on leachate solutions

CV analysis of the 121 CEC and leachate solution was conducted at 358 K (electrodeposition conditions) to determine the solvent stability and Ni reduction potential. CV was performed using GC as the WE, Pt as the CE, and a Ag wire as the RE at a scan rate of 20 mV s^{-1} (Fig. 3a). The ferrocene redox couple (Fc/Fc^+) was used as a known reference to determine the potential of the Ag wire electrode. The CV of 10 mM ferrocene in 121 CEC (Fig. S8a†) showed an oxidation peak at 0.42 V *versus* the Ag wire. The CV of 121 CE recorded at RT shows an ESW of 2.55 V *vs.* Ag wire, with an onset cathodic and anodic potential of −1.25 V and 1.3 V *vs.* Ag wire, respectively (Fig. S8b†). The increase in current near 1.3 V *vs.* Ag wire was attributed to chlorine evolution.[57,58] At 358 K, ESW is reduced to 1.41 V, with the onset cathodic and anodic potentials of −0.79 V and 0.6 V *vs.* Ag wire, respectively (Fig. 3a, black line). The CV response of the leachate solution showed an irreversible reaction with a distinct anodic peak around 0.2 V, while no clear cathodic peak was observed (Fig. S9a,† blue line).

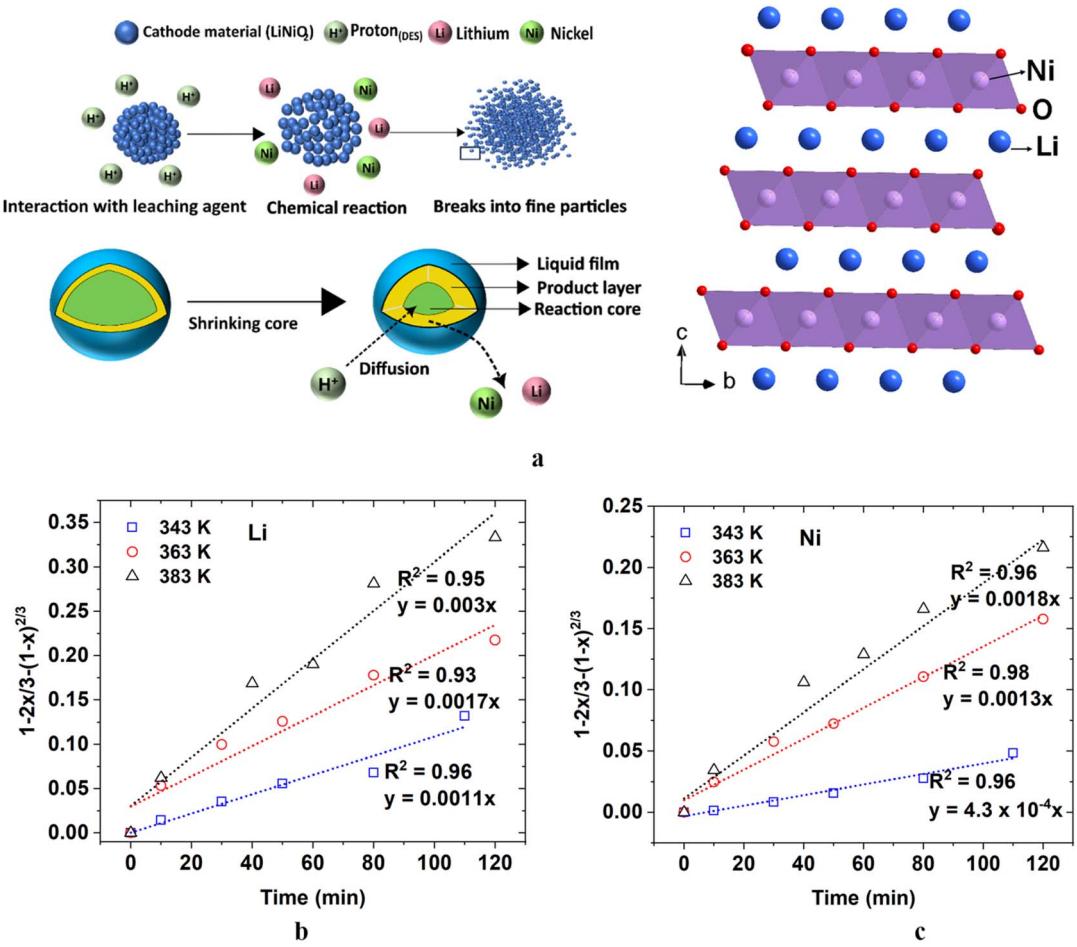

Fig. 2 (a) Proposed leaching mechanism and crystal structure of the cathode material; (b) leaching kinetics model of Li at different temperatures (2 h); (c) leaching kinetics model of Ni at different temperatures (2 h).

CV measurements were performed on the leachate solution at various cathodic end potentials (E_c), from −0.6 V to −1.6 V *vs.* Ag wire (Fig. 3b and S9a†), to understand the Ni^{2+} reduction potentials. Fig. 3c shows only the cathodic segments of these curves and illustrates the variation in the slope of the cathodic peak with different end potentials. At −0.6 V, the minimal cathodic current indicates negligible Ni^{2+} reduction; subsequently, no anodic peak was observed upon reversal. In contrast, at −1 V, nickel reduction is dominant with minimal interference from the onset of DES degradation (Fig. 3b and c). A consistent increase in the anodic peak from −1 V provides indirect evidence of nickel reduction, indicating increased nickel deposition during the cathodic process, which is subsequently oxidized during the anodic sweep (Fig. 3b). Extending the potential to more negative values (beyond −1.4 V) further enhanced current density (−0.28 mA cm^{-2}), indicating a favorable reduction of Ni^{2+} to Ni; however, at E_c = −1.6 V, a slight reduction in the anodic peak intensity was observed. This suggests that accelerated DES degradation (Fig. 3c, blue shaded region) and additional side reactions such as the hydrogen evolution reaction (HER), introduce bubbles at the electrode surface, contribute to passivation, and limit nickel deposition, resulting in reduced oxidation. Due to the increased side reactions, the Ni electrodeposition potential range was considered from −1 V to −1.6 V *vs.* Ag wire. A hysteresis loop was evident during the reverse sweep, suggesting overpotential-induced nucleation, growth, and surface changes due to the electrodeposition (Fig. 3b, inset).[57,58]

In Fig. 3c, between the onset of Ni^{2+} reduction (−0.5 V) and the potential where the DES remains electrochemically stable (−0.8 V), the slope is consistent (pink shaded triangle; I). Up to −1.0 V (green dotted triangle; II), minor deviations in the slope are attributed to the early onset of DES degradation. At potentials more negative than −1.4 V (brown shaded region; III), the slope variation becomes more pronounced due to electrochemical DES degradation and the HER catalyzed due to the freshly deposited nickel (Fig. S15†). Passivation effects become more evident in consecutive CV cycles, where a shift in the cathodic slope and a decrease in anodic peak intensity indicate surface modifications of the WE (Fig. S9b and d†).

The leaching reaction generates water as a byproduct (eqn (3)) due to the cleavage of metal-oxide bonds and hence, water content can vary between the batches.[25,36,38] In addition, the DES is hydrophilic; hence, the leachate was treated with 2 mL (6 wt%) water to assess the effect of water on the electrochemical response (Fig. S9c†). Although water narrows the

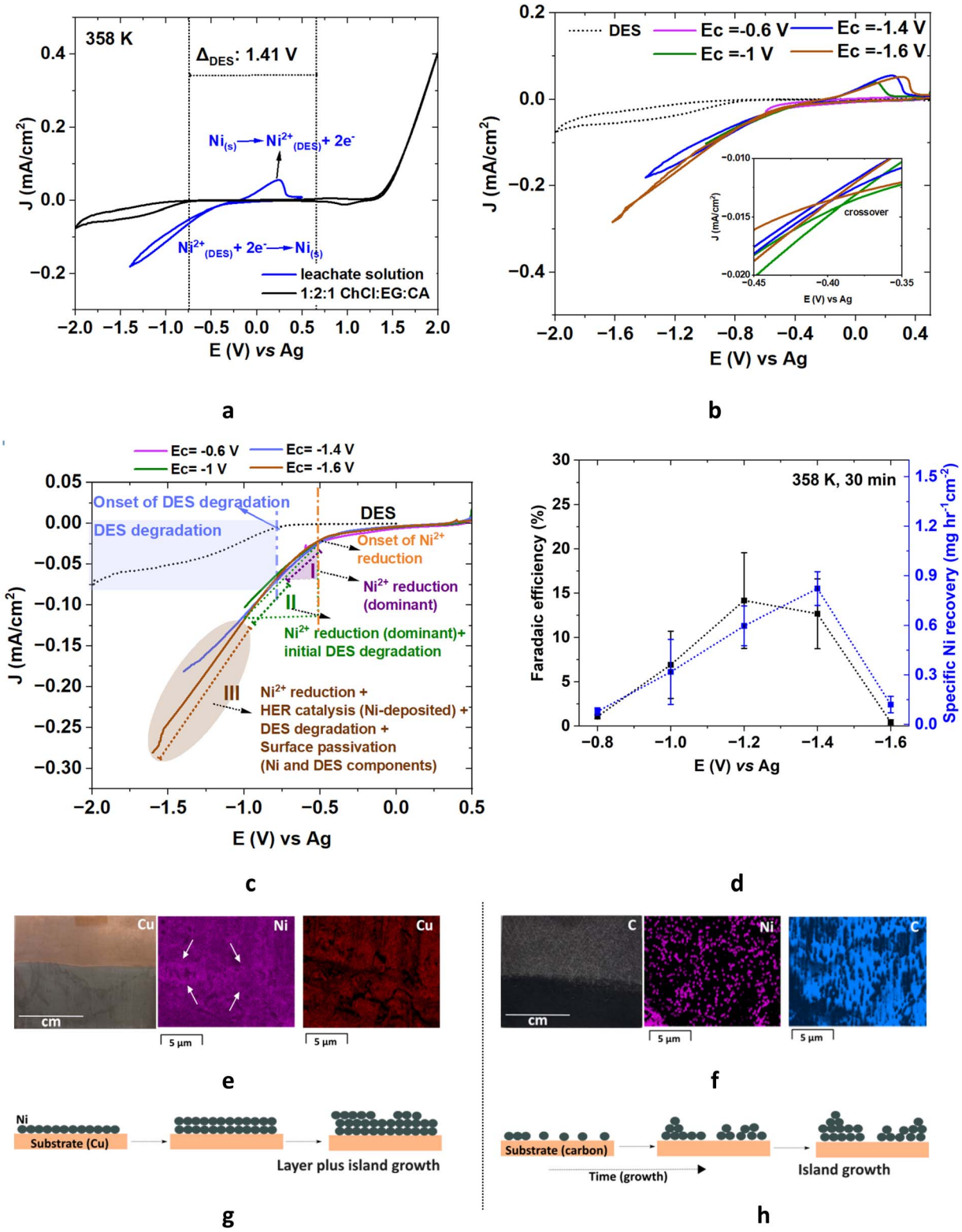

Fig. 3 (a) CV of the leachate solution (blue line) and 121 CEC (blank, black line) at 358 K. The sweep direction is from 0.5 V. WE: GC; CE: Pt; RE: Ag wire; scan rate: 20 mV s^{-1}. (b) CV of 121 CEC and the corresponding leachate solution at 358 K with different end cathodic potentials (E_c), ranging from −0.6 V to −1.6 V. (c) Cathodic scan of CV curves scanned from 0.5 V to the respective end potentials highlighting different reactions. Black dotted line: DES without metal species; blue shaded region: DES degradation; pink shaded triangle and pink line: slope measured between the onset of Ni^{2+} reduction and before DES degradation begins along with the corresponding reactions; green open triangle and green line: slope measured between the onset of Ni^{2+} reduction and the initial DES degradation phase along with the corresponding reactions; brown shaded region and brown line: slope variations due to the interplay of multiple electrochemical reactions. (d) Effect of applied potential on FE and R_{Ni} at

electrochemical window, it reduces viscosity and enhances diffusion, resulting in an increased anodic peak intensity that implies improved reduction kinetics. Even small water uptake between cycles and effects of prior cycle degradation, variability in electrode cleaning, solution handling, and stirring can alter the electrochemical profile. A quantitative analysis of these factors is beyond the scope of this study.

Moreover, previous studies suggest that the DES components, such as ChCl and EG, undergo chemical changes under leaching conditions to aid the metal extraction.[20,34,37,59] These species can alter the Ni^{2+} reduction kinetics and affect charge transfer at different potentials. These combined effects—DES degradation, water absorption, metal deposition, hydrogen evolution, and consequent surface passivation—govern the observed slope variations as the cathodic potential becomes more negative. Hence, the slope comparison should be considered only for the regions where the DES is electrochemically stable (region I, Fig. 3c).

Chronoamperometry measurements were conducted in leachate solutions at varied temperatures utilizing a GC (0.071 cm^2) as the WE, Pt as the CE, and a Ag wire as the RE. The diffusion coefficient of Ni for different temperatures is determined using the Anson equation (eqn (9), ESI†) and calculated to be 8×10^{-10}, 4×10^{-9}, and 3×10^{-7} cm^2 s^{-1} at 328 K, 358 K, and 388 K, respectively.[60,61] The diffusion coefficient of Ni in the DES is typically 10^{-8} and 10^{-7} for 1:2 ChCl:urea and 12 CE, respectively.[57,62] The lower diffusion coefficient is attributed to the higher viscosity of 121 CEC (2400 mPa s) at 298 K, compared to 1:2 ChCl:urea (950 mPa s) and 12 CE (37 mPa s), as is apparent from the Stoke–Einstein equation $\left(D = \left(\frac{K_B T}{6\pi\mu R_{hyd}}\right)\right)$.[57,62]

2.4 Electrodeposition of nickel

The electrodeposition of Ni from a leachate solution (121 CEC) was conducted in a 3-electrode cell setup. The preliminary studies on the choice of electrodes are described in the ESI (Section S4, Fig. S10).† The choice of a stable CE directly impacts the success of the electrodeposition. Dimensionally stable anodes (DSAs) have been widely used in the chlor-alkali industry, as they offer longer shelf life and high mechanical, thermal, and chemical stability in acidic media compared to traditional graphite.[63] Considering the requirements of thermal and electrochemical stability, a DSA—ruthenium and iridium oxide coated on titanium (RTI)—was chosen as the CE.[63]

The electrodeposition process was carried out at different temperatures (298–388 K), applying varied constant potentials (−0.7 V to −1.6 V *vs.* Ag wire) for different durations (10–90 min). Initially, an electrodeposition temperature of 358 K was chosen, close to the optimized leaching temperature, to minimize energy conversion requirements in an industrial continuous process.

2.4.1 Effect of the reduction potential and working electrode. The reduction potential has a vital role in the electrodeposition process. A more negative reduction potential could lead to higher current density and recovery rate; however, it could also degrade the DES components and induce side reactions such as the HER, affecting selectivity and faradaic efficiency.

Case 1: Cu sheet as the WE; RTI as the CE. When the Cu sheet was used as the WE and RTI as the CE, at 358 K for 30 min, visible Ni deposition was seen on the Cu sheet at varied potentials from −0.7 V to −1 V *vs.* Ag wire (Fig. S11†). However, the mass difference of the Cu sheet indicated that Cu undergoes leaching at 358 K. This observation was further supported by altering the deposition time to 10 and 60 min. A slight positive mass difference was obtained after 10 min of deposition (FE < 5%, −0.7 V *vs.* Ag wire), while negative mass differences were observed after 30 and 60 minutes, indicating leaching over time. Lowering the electrodeposition temperature to 328 K and 298 K did not result in any apparent deposition, which could be attributed to the transport limitations.

Case 2: carbon paper as the WE; RTI as the CE. Carbon paper was used as the WE at 358 K for 30 min, with applied potentials ranging from −0.8 V to −1.6 V *vs.* Ag wire. Unlike the Cu sheet as the WE, no significant Ni deposition was observed at lower reduction potentials on the carbon substrate (<−1 V *vs.* Ag wire). This indicates that a higher potential is required for electrodeposition on carbon compared to the Cu sheet (deposition seen for −0.7 V *vs.* Ag wire).[64] Fig. 3d shows the FE and R_{Ni} for different reduction potentials. FE and R_{Ni} increase with an increase in negative potentials, as electrical potential drives metal deposition. The highest FE and R_{Ni} were obtained for −1.4 V *vs.* Ag wire with 14 ± 4% and 0.8 $mg^{-1}cm^{-2}$ ±0.1, respectively (Fig. 3d). The reduction in FE and R_{Ni} for the reduction potential at −1.6 V *vs.* Ag wire can be attributed to side reactions such as the HER and solvent degradation at a high negative potential.

Scanning Electron Microscopy-Energy Dispersive X-ray Spectroscopy (SEM/EDX) confirms the successful deposition of Ni on Cu and carbon substrates using RTI as the CE (Fig. 3e and f). The deposited Ni on the Cu sheet is visually identified as grey (Fig. 3e), whereas it is difficult to locate on carbon due to its black nature. The substrate has significant importance in the microstructure of the Ni metal deposited. The morphology of Ni deposition is found to be layer plus island mode, whereas the carbon exhibits a different growth mechanism, demonstrating a typical island growth mode. The EDX mapping shows the distribution of nickel across the Cu sheet (Fig. 3e and S13†) and carbon substrate (Fig. 3f and S14†). Fig. 3g reveals instances where Ni grows on top of the existing Ni surface, indicated by white arrows, suggesting a multilayer formation attributable to layer-plus-island mode.[15] The growth mode of Ni on Cu and the carbon substrate depends on the interaction energy between

358 K for 30 min on a carbon substrate. WE: carbon paper; CE: RTI; RE: Ag wire. (e) Optical image and EDX elemental map of Ni on a Cu substrate (−1 V *vs.* Ag, at 358 K, 30 min). (f) Optical image and EDX elemental map of Ni on a carbon substrate (−1 V *vs.* Ag wire, at 358 K, 30 min). (g) Schematic of layer-island growth and (h) island growth. The error bars represent standard errors calculated from three independent experiments.

Table 1 Crystallographic parameters and surface segregation energy for Ni recovery on different substrates

Parameter	Cu	Carbon
Lattice constant (Å)	3.61 (Ni: 3.52)	2.46 (Ni: 3.52)
d-spacing (Å)	2.087 (Ni: 2.034)	3.35 (graphene) (Ni: 2.034)
Surface segregation energy (eV)	0.17	N/A
Interaction strength	Strong	Weak

the metal adatoms and the substrate (Fig. 3e–g). If Ni has weak interactions with the substrate atoms, it tends to form island mode (Fig. 3f–h). However, if Ni has strong interactions with the substrate, it spreads over the substrate surface and includes a layer or layer-island growth mode (Fig. 3e). Although the Cu substrate has a more vital interaction with Ni, due to the stability issue of Cu, in the DES solution, carbon is selected as a WE from the deposition studies for further optimization. Identifying the appropriate substrate can significantly influence the success of electrodeposition.

Two main factors affecting Ni recovery on these substrates can be explained using crystallographic parameters and surface segregation energy (Table 1). The lattice constant of Ni is 3.52 Å, while that of Cu is 3.61 Å.[65] The small lattice mismatch allows for coherent growth of Ni on Cu, minimizing strain and promoting better adhesion. The *d*-spacing between the (111) planes of Ni and Cu are 2.034 Å and 2.087 Å, respectively, illustrating their compatibility.[15,66] However, carbon does not have a lattice structure compatible with Ni as Cu does. The lattice constant for graphene is about 2.46 Å for the hexagonal unit cell, and the *d*-spacing for graphene planes is approximately 3.35 Å.[67] Despite the lattice mismatch, the large surface area of the carbon, combined with the strong interaction between Ni and the π-electrons of graphene, enhances adhesion and nucleation. Surface segregation energy measures the tendency of atoms in an alloy to migrate from the bulk to the surface. The surface segregation energy of Ni on Cu is 0.17 eV, indicating moderate anti-segregation.[68] Although specific Ni data on carbon are unavailable, similar studies suggest weaker interactions due to more significant size mismatches and weaker binding energies.

Carbon paper provides better chemical stability due to its inert nature. However, the lack of lattice mismatch with Ni requires more negative potential for sufficient nucleation and growth.[15]

2.4.2 Effect of electrodeposition temperature and time. The effect of electrodeposition temperature (298–388 K) and time (10–90 min) on Ni recovery using a carbon substrate was examined (Fig. 4). Fig. 4a shows that the R_{Ni} increases with temperature. At 300–320 K, minimal electrodeposition occurs, likely due to transport limitations from the viscosity of the leachate solution. However, above 350 K, the R_{Ni} increases from 0.8 $\pm$ 0.1 to 1.3 $\pm$ 0.2 mg h^{-1} cm^{-2} as the diffusion of metal ions to the substrate increases. As temperature increases, the viscosity of the DES is reduced, enhancing Ni ion diffusion to the cathode and reducing the energy barrier for metal deposition. The diffusion coefficient of Ni at different temperatures is also in agreement. However, we do not observe significant improvement in FE, with the FE values of 16 $\pm$ 4% and 14 $\pm$ 2% at 358 and 388 K, respectively. The electrodeposition temperature above 388 K was avoided to ensure solvent stability (Fig. S4†).

The effect of electrodeposition time (10–120 min) on Ni recovery using a carbon substrate was investigated at 388 K (Fig. 4b). Unlike the Cu sheet as the WE, a 10-min electrodeposition time showed no significant deposition on the carbon substrate. However, when the time was increased to 30 min, FE and R_{Ni} values of 14 $\pm$ 2% and 1.3 mg h^{-1} cm^{-2} $\pm$ 0.2 were obtained, respectively. The increase in R_{Ni} from 10 to 30 min can be attributed to the diffusion and availability of active sites on the substrate for electrodeposition.

Prolonging deposition to 60 and 90 min decreased R_{Ni} to 0.98 $\pm$ 0.2 and 0.6 $\pm$ 0.3, respectively. This decrease is likely due to deposited Ni, which might catalyze side reactions such as the HER, as evidenced by bubble formations (Fig. S14†). CV on the 121 CEC with Ni as the WE, Pt as the CE, and Ag as the RE confirmed the occurrence of the HER (Fig. S15†), leading to a notable decrease in ESW compared to using GC as the WE. Similar ESW reductions were observed with Ni in 12 CE, indicating Ni's catalytic role in solvent reduction and the HER.[62] To mitigate this side reaction on an industrial scale, periodic removal of Ni from the electrode surface is suggested.

Fig. 4c illustrates the Ni electrodeposition process, which involves three key steps: (i) potential-induced Ni ion transport from the leachate to the cathode, (ii) electrochemical reduction at the cathode ($Ni^{2+} + 2e^- \rightarrow Ni_{(s)}$) and competing side reactions ($H^+ + 2e^- \rightarrow H_{2(g)}$). At the anode ($2Cl^- \rightarrow Cl_2 + 2e^-$), oxidation of EG and CA to glycolic acid or small organic acids and CO_2 at very high potential (0.6 to 1 V *vs.* RHE) can also occur as side reactions[72,73] and (iii) nucleation and growth (Fig. 4d). Increasing temperature enhances Ni diffusion to the cathode, with 388 K identified as the optimal temperature considering both R_{Ni} and DES thermal stability.

Under the applied potential, Ni^{2+} ions reduce to Ni at the cathode. Over time, R_{Ni} decreases due to the competition between faradaic reactions (Ni deposition) and side reactions (HER), with deposited Ni acting as a catalyst for the HER (Fig. 4e). SEM-EDX reveals the formation of oxide layers on Ni when exposed to air (Fig. S13†).

In addition, lithium can be recovered from the leachate by precipitation (pH $\sim$ 11) with sodium carbonate to form lithium carbonate (Li_2CO_3) or by electroplating based on the DES ESW.[74,75]

2.4.3 Effect of viscosity. Viscosity plays a critical role in determining the performance of DESs, especially in electrochemical recovery. Although increasing temperature reduces viscosity, it can also lead to thermal degradation, as observed from TGA, and promote electrochemical side reactions, such as the HER, along with substrate instability during

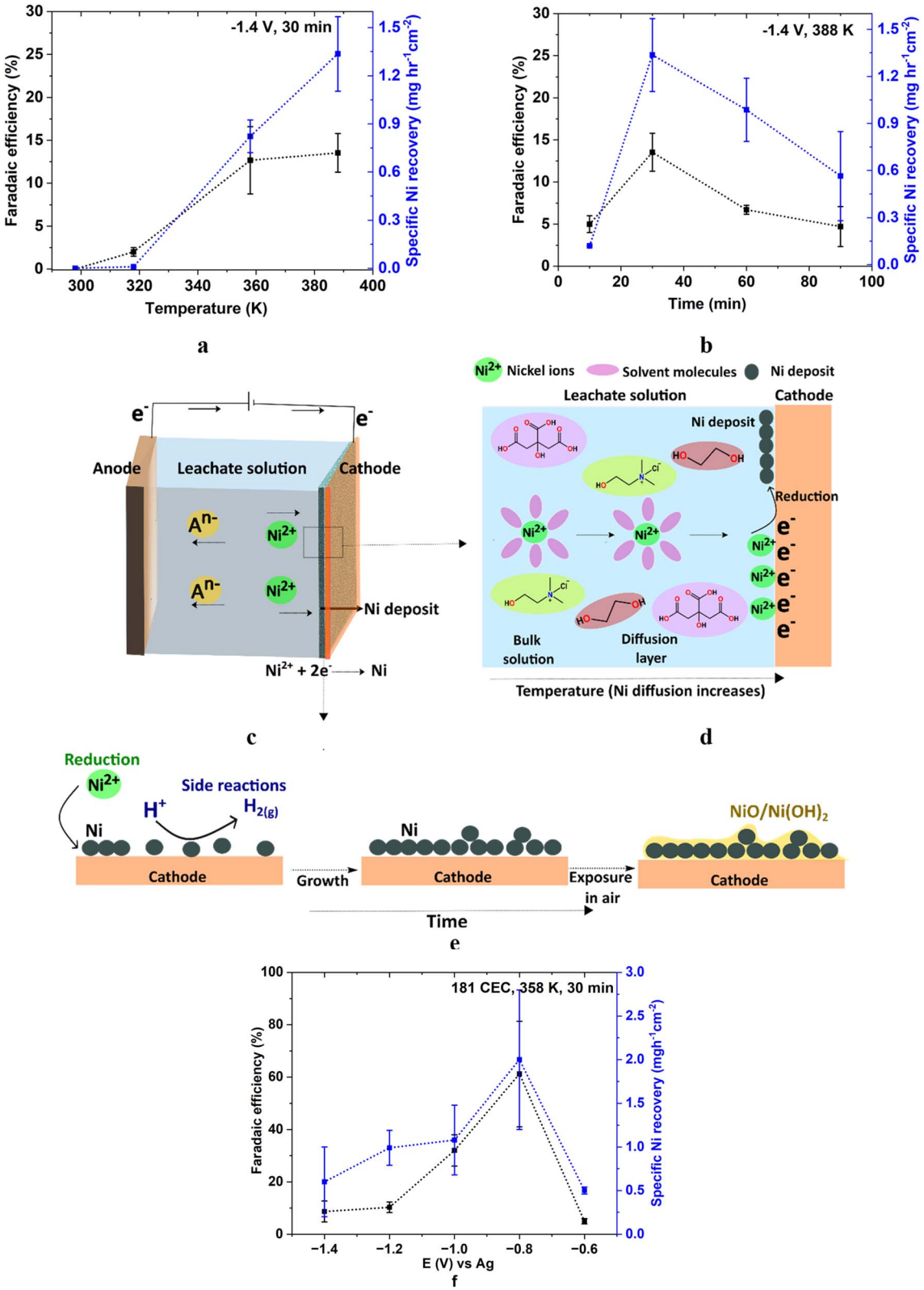

Fig. 4 (a) Effect of temperature on FE and R_{Ni} at −1.4 V *vs.* Ag wire, 30 min. (b) Effect of time on FE and R_{Ni} at −1.4 V *vs.* Ag wire, 388 K; WE: carbon paper; CE: RTI; RE: Ag wire. (c–e) Overall electrodeposition mechanism. (f) Effect of applied potential on FE and R_{Ni} at 358 K for 30 min on a carbon substrate from 181 CEC (reduced viscosity; diluted from 121 CEC leachate solution). WE: carbon paper; CE: RTI; RE: Ag wire. The error bars represent standard errors calculated from three independent experiments.

Table 2 (a) Viscosity, leaching, and electrochemical recovery efficiencies for various cathode materials using DESs, (b) viscosity, leaching, and non-electrochemical/no-recovery methods for organic and non-organic-acid DESs

Cathode materials	DES	Viscosity (mPa s) at 20 °C (ref. 69)	LE (%)	Leaching conditions	Recovery of metals from leachate solution (FE%)	Ref
(a) Electrochemical recovery						
LCO	1:2 ChCl:EG	37	Co: 100	0.1 g/5 g 160 °C, 42 h	Electrodeposition Co: 20% (20 °C, 40 min) Co: 50% (20 °C, 100 min)	29
LCO	1:5 ChCl:EG	∼30	Co: 100	0.1 g/5 g 160 °C, 48 h	Electrodeposition Co: 80% (50 °C, 40 min)	29
LCO	1:2 ChCl:urea	750	Co: 100; Li: 100	0.1 g/5 g 170 °C, 4 h	Electrodeposition Co: 54% (94 °C, 60 min)	15
NMC	1:2 ChCl:EG	37	Li: 70.80; Co: 31.71; Ni: 6.65; Mn: 60.16	0.02 g/5 g; 180 °C; 24 h	Electrodeposition Co: N/A	21
LNO	1:2:1ChCl:EG:CA	2400 191 (85 °C)	Li: 100; Ni: 98	0.1 g/5 g 90 °C; 5 h	Electrodeposition Ni: 14% (115 °C, 30 min)	This work
LNO	1:8:1 ChCl:EG:CA	430 20 (85 °C)	Li 92; Ni: 83	0.1 g/5 g 90 °C, 3 h	Electrodeposition Ni: 65% (85 °C, 30 min)	This work
(b) Alternative methods or no metal recovery from leachate						
Organic-acid based DES						
NMC	1:2:1 ChCl:EG:CA	2400	Li: 94; Mn: 99; Co: 99; Ni:85	0.1 g/5 g; 90 °C; 24 h	N/A	This work
LCO	1:1 ChCl:CA	9126	Co: 99.6	0.1 g/5 g; 60 °C	Solvent extraction	22
LCO	ChCl:oxalic acid	231	Co: 19.6	0.1 g/5 g; 60 °C	N/A	22
LCO	ChCL:malic acid	N/A	Co: 81.2	0.1 g/5 g; 60 °C	N/A	22
LCO	ChCl:malonic acid	721	Co: 24	0.1 g/5 g; 60 °C	N/A	
NMC	1:1 ChCl:tartaric acid	6840 (water 1 w/w%)	Li: 96.0; Co: 97.1; Ni: 98.0; Mn: 96.7	0.1 g/5 g; 70 °C; 12 h	Antisolvent crystallization	12
NMC	1:2 ChCl:lactic acid + water	N/A	Li: 96.2; Co: 98; Mn: 99; Ni: 98.9	0.1 g/2.5 g; 50 °C; 1 h	Precipitation	70
Nonorganic-acid based DES						
LNO	1:2 ChCl:EG	37	Ni: <5, Li: 20	0.1 g/5 g; 90 °C, 12 h	N/A	This work
NMC	1:2 ChCl:EG	37	Li: 70.80; Co: 31.71; Ni: 6.65; Mn: 60.16	0.02 g/5 g; 180 °C; 24 h	N/A	71
NMC	1:2 ChCl:urea	750	Li < Mn < Ni < Co: >95	180 °C; 24 h	Precipitation	13

electrodeposition, particularly for copper. To address these challenges, the viscosity of the DES was modified by adjusting the molar ratio of components to make 181 CEC. At 85 °C, the viscosity of 181 CEC was reduced to approximately one-eighth of 121 CEC (22 mPa s for 181 CEC compared to 191 mPa s for 121 CEC) (Fig. S16†). The leaching of metals performed using 181 CEC shows 92% LE for Li and 82% for Ni at 363 K in 2 h (Fig. S17†).

Electrodeposition studies were performed at 358 K for 30 minutes on a carbon substrate, using a diluted 121 leachate solution to which a fourfold molar ratio of EG was added (resulting in a 181 CEC ratio). At −0.8 V *vs.* Ag wire, FE increased to 65% (Fig. 4f). The improved FE for 181 CEC at lower potentials is attributed to enhanced mass transport of Ni ions. SEM-EDX confirms the presence of Ni (Fig. S18†). Overall, the improvement in FE arises from multiple factors: reduced viscosity without requiring high temperatures (*e.g.*, 115 °C as in 121 CEC), which minimizes side reactions such as the HER and thermal degradation, and the use of lower applied potentials (−0.8 V for 181 CEC *vs.* −1.4 V for 121 CEC), also reduce electrochemical degradation of DES components. The oxidation of EG and CA is prone to happen at high potential (0.6–1 V *vs.* RHE), degrading to small organic acids.[72,73]

Table 2 compares DES systems and highlights the interplay between viscosity, LE, and electrochemical recovery (FE). The low-viscosity DES, such as 12 CE, provides good FE but often requires harsh leaching conditions, leading to thermal degradation of the DES (Table 2, a).[29]

The organic acid-based DES is crucial for achieving high LE under mild conditions; however, their high viscosities often limit mass transport (Table 2, b), which is critical for the electrochemical recovery of metals. Often, water is used to decrease the viscosity. However, water reduces electrochemical stability, promoting HER side reactions during electrodeposition. The superior performance of 181 CEC demonstrates the critical role of viscosity reduction in achieving an optimal balance between efficient leaching and electrochemical recovery (Table 2, a). This highlights viscosity as a key parameter for tailoring DESs to meet specific leaching and electrochemical recovery requirements.

2.6 Reusability of the DES

To assess the reusability of the DES, the same leaching and electrodeposition conditions were applied to the DES over multiple cycles without adding new cathode materials. This method isolates the DES's inherent stability and reusability, providing a clearer understanding of its behavior under thermal and electrochemical exposure with repeated use. Given the absence of Ni electroactive species at −1.4 V *vs.* Ag wire, the DES is expected to undergo more severe side reactions.

LE was measured after each cycle of leaching and electrodeposition for 3 cycles. The LE for both metals remained above 90% after two cycles, indicating high stability (Fig. 5). In Cycle 0, the initial LE for both Li and Ni was 99 ± 2% and 93 ± 5%, respectively. Given the standard error in cycles 1 and 2, LE consistently stayed above 90%, indicating that the DES retains relatively high

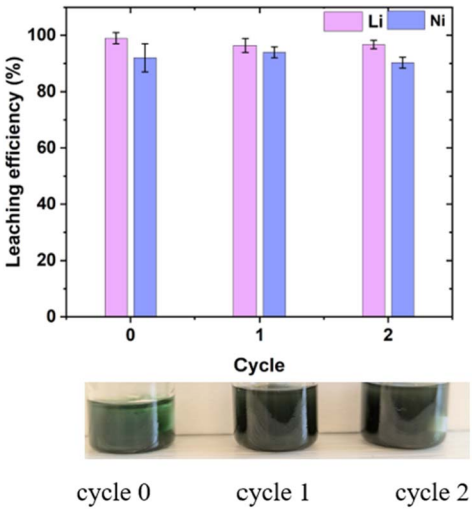

Fig. 5 LE of Li and Ni over three cycles using 121CEC. Cycle 0 represents the LE before electrodeposition, along with the photos of the leachate solution. Cycles 1 and 2 represent the LE after each subsequent leaching (363 K, 24 h) and electrodeposition. The error bars represent standard errors calculated from three independent experiments.

efficiency despite some degradation. The slight drop in LE can be attributed to side reactions and the electrochemical oxidation of EG and CA to glycolic acid or small organic acids and CO_2 at very high potentials (0.6 to 1 V *vs.* RHE).[72,73] Future work should focus on developing DES formulations with improved thermal and electrochemical stability to minimize side reactions and extend its usability over more cycles.

2.7 Feasibility of the T-DES in LIB recycling

2.7.1 Performance with the simulated black mass. To evaluate the effectiveness of the T-DES in metal leaching, a simulated black mass containing a PVDF binder, carbon, and LNO was prepared, as the industrial black mass was inaccessible to us. SEM images reveal the layered structure of pure LNO, while in the simulated black mass, LNO is covered with PVDF (Fig. S19†). Despite this, the LE remained high at 99 ± 9% for Li and 90 ± 6% for Ni for the leaching with the simulated black mass at 363 K, 24 h. Impurities such as Al and Cu from the current collector may affect LE in practical recycling scenarios, requiring optimization of reagent concentrations and process conditions to maximize Ni recovery. The distinct reduction potentials of other LIB components (Li: −3.04 V, Al: −1.66 V, Cu: 0.34 V, Ni: −0.25 V *vs.* SHE) make it unlikely that other impurities such as Al and Cu interfere with the selective electrodeposition of Ni under these conditions.[76]

2.7.2 Application to other cathode materials. To evaluate the effectiveness of the T-DES in metal leaching of other cathode materials such as NMC, leaching was performed under the following conditions: 363 K for 24 h and a solid/liquid (S/L) ratio of 20 mg g^{-1}. After the leaching, the color of the DES changed from transparent to blue, which can be attributed to the presence of cobalt. The leaching efficiencies for individual

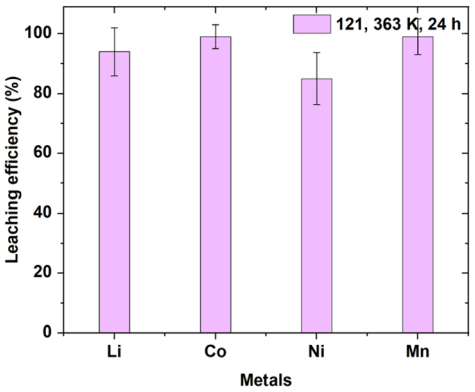

Fig. 6 LE of metals from the NMC cathode material using 121CEC at 363 K for 24 h. The error bars represent standard errors calculated from three independent experiments.

metals were determined to be 94 ± 8% for Li, 99 ± 6% for Mn, 85 ± 6% for Ni, and 99 ± 3% for Co, respectively (Fig. 6). Optimization of leaching conditions and metal recovery processes are beyond the scope of this study and will be addressed in future work. These findings demonstrate the potential of the T-DES as an efficient leaching agent for broader applicability for other LIB cathode materials under mild conditions. Previous techno-economic analyses comparing DES-based and conventional hydrometallurgical technologies highlight several advantages of the DES, such as low-concentration, eco-friendly leaching agents, reduced chemical expenses, and low toxicity, which streamline waste management.[41]

3 Conclusions

This work introduces a novel approach for recovering Li and Ni from LNO materials using a T-DES. The design of the T-DES was based on three critical criteria: minimizing transport limitations through viscosity control, utilizing acidic HBDs for effective leaching, and ensuring electrochemical stability. The T-DES demonstrated improvements in terms of viscosity (190 mPa s at 358 K), LE (>95%, 70–105 °C), and electrochemical stability (2.05 V *vs.* Ag wire) compared to the corresponding B-DES, which had limitations in leaching ability or viscosity, restricting its applications in LIB recycling.

Electrochemical studies demonstrated the feasibility of Ni electrodeposition from the leachate solution and highlighted the importance of substrate stability, applied potential, electrodeposition temperature, and time. The choice of substrate notably impacted the electrodeposition process. Carbon substrates were preferred over Cu due to their chemical stability, although they required a higher potential (−1.4 V *vs.* Ag wire) than Cu sheets (−0.7 V *vs.* Ag wire). The optimal conditions for Ni electrodeposition from the 121 CEC leachate solution were identified as −1.4 V, 110 °C for 30 min, resulting in an estimated Ni deposition rate of 1.33 ± 0.2 mg h^{-1} cm^{-2}.

By modifying the molar components of the DES to 181 CEC, viscosity was significantly reduced to 20 mPa s (85 °C) *vs.* (190 for 121 CEC), which enhances ion diffusion and allows electrodeposition at an applied potential of −0.8 V *vs.* Ag (65%, 30 min). This increase in FE is a combination of factors: viscosity reduction, achieved without relying on high temperatures, which can otherwise cause thermal degradation, reduce electrochemical stability, and promote side reactions. This study underscores the role of viscosity in designing the DES for leaching and electrodeposition.

Additionally, the T-DES was also effective for other cathode materials such as NMC, achieving high LE values of 94 ± 8% for Li, 99 ± 6% for Mn, 85 ± 6% for Ni, and 99 ± 3% for Co at 90 °C (24 h). Overall, this study provides valuable insights into developing a sustainable approach for recovering critical metals from LIB waste, contributing to the broader goal of sustainable battery recycling.

Data availability

The data supporting this article have been included as part of the ESI.†

Author contributions

Dr Suchithra A. Sahadevan: data curation, formal analysis, investigation, methodology, validation, visualization, writing – original draft, writing – review & editing. Dr Mohamed Shahid: investigation, methodology, validation, writing – original draft. Dr Shrihari Sankarasubramanian: conceptualization, funding acquisition, writing – review & editing, supervision, validation, project administration, resources. Dr Vijay Ramani: conceptualization, funding acquisition, writing – review & editing, supervision, validation, project administration, resources.

Conflicts of interest

There are no conflicts to declare.

Acknowledgements

The authors acknowledge the McKelvey School of Engineering, Washington University in St. Louis, and the Roma B. & Raymond H. Wittcoff Distinguished University Professorship. We gratefully acknowledge access to instrumentation from the WashU Chemical and Environmental Analysis Facility (CEAF), Materials Characterization Facility in the Institute of Materials Science & Engineering (IMSE), and MEMS Shared Instrument Group for the rheometer use. M. S. and S. S. acknowledge support from the University of Texas at San Antonio. We thank Prof. Alan Wittington for using his rheometer.

References

1 X. Zheng, Z. Zhu, X. Lin, Y. Zhang, Y. He, H. Cao and Z. Sun, *Engineering*, 2018, **4**, 361–370.
2 X. Zheng, W. Gao, X. Zhang, M. He, X. Lin, H. Cao, Y. Zhang and Z. Sun, *Waste Manage.*, 2017, **60**, 680–688.

3 H. Wang, K. Huang, Y. Zhang, X. Chen, W. Jin, S. Zheng, Y. Zhang and P. Li, *ACS Sustainable Chem. Eng.*, 2017, **5**, 11489–11495.
4 E. Gratz, Q. Sa, D. Apelian and Y. Wang, *J. Power Sources*, 2014, **262**, 255–262.
5 J. Neumann, M. Petranikova, M. Meeus, J. D. Gamarra, R. Younesi, M. Winter and S. Nowak, *Adv. Energy Mater.*, 2022, **12**, 2102917.
6 M. Chen, X. Ma, B. Chen, R. Arsenault, P. Karlson, N. Simon and Y. Wang, *Joule*, 2019, **3**, 2622–2646.
7 Y. Yao, M. Zhu, Z. Zhao, B. Tong, Y. Fan and Z. Hua, *ACS Sustainable Chem. Eng.*, 2018, **6**, 13611–13627.
8 S. Ashoka Sahadevan, X. Xiao, Y. Ma, K. Forsberg, R. T. Olsson and J. M. Gardner, *Mater. Chem. Front.*, 2023, **7**, 1374–1384.
9 L. Brückner, J. Frank and T. Elwert, *Metals*, 2020, **10**, 1107.
10 C. Liu, J. Lin, H. Cao, Y. Zhang and Z. Sun, *J. Cleaner Prod.*, 2019, **228**, 801–813.
11 V. Velázquez-Martínez, R. Santasalo-Aarnio and S. Guerrero, *Batteries*, 2019, **5**, 68.
12 C. Ma, M. Svärd and K. Forsberg, *Resour., Conserv. Recycl.*, 2022, **186**, 106579.
13 S. Wang, Z. Zhang, Z. Lu and Z. Xu, *Green Chem.*, 2020, **22**, 4473–4482.
14 Z. Xu, H. Shao, Q. Zhao and Z. Liang, *JOM*, 2021, **73**, 2104–2110.
15 H. Wang, M. Li, S. Garg, Y. Wu, M. Nazmi Idros, R. Hocking, H. Duan, S. Gao, A. J. Yago, L. Zhuang and T. E. Rufford, *ChemSusChem*, 2021, **14**, 2972–2983.
16 Z. Yuan, H. Liu, W. F. Yong, Q. She and J. Esteban, *Green Chem.*, 2022, **24**, 1895–1929.
17 E. L. Smith, A. P. Abbott and K. S. Ryder, *Chem. Rev.*, 2014, **114**, 11060–11082.
18 D. O. Abranches and J. A. P. Coutinho, *Curr. Opin. Green Sustainable Chem.*, 2022, **35**, 100612.
19 R. K. Ibrahim, M. Hayyan, M. A. AlSaadi, S. Ibrahim, A. Hayyan and M. A. Hashim, *J. Mol. Liq.*, 2019, **276**, 794–800.
20 M. Svärd, C. Ma, K. Forsberg and P. G. Schiavi, *ChemSusChem*, 2024, **17**, e202400410.
21 M. K. Tran, M.-T. F. Rodrigues, K. Kato, G. Babu and P. M. Ajayan, *Nat. Energy*, 2019, **4**, 339–345.
22 N. Peeters, K. Binnemans and S. Riaño, *Green Chem.*, 2020, **22**, 4210–4221.
23 A. Zhu, X. Bian, W. Han, D. Cao, Y. Wen, K. Zhu and S. Wang, *Resour., Conserv. Recycl.*, 2023, **188**, 106690.
24 J. Wang, Y. Lyu, R. Zeng, S. Zhang, K. Davey, J. Mao and Z. Guo, *Energy Environ. Sci.*, 2024, **17**, 867–884.
25 Z. Yuan, H. Liu, W. F. Yong, Q. She and J. Esteban, *Green Chem.*, 2022, **24**, 1895–1929.
26 Y. Wen, X. He, S. Di, K. Liu, D. Li and J. Du, *J. Environ. Chem. Eng.*, 2023, **11**, 110979.
27 B. Lu, R. Du, G. Wang, Y. Wang, S. Dong, D. Zhou, S. Wang and C. Li, *Environ. Res.*, 2022, **212**, 113286.
28 I. N. Perera, J. M. Pringle, K. Periyapperuma, A. Somers, A. Siriwardana, G. Pozo and C. Pozo-Gonzalo, *J. Electrochem. Soc.*, 2023, **170**, 052503.
29 M. Shahid, S. Ashoka Sahadevan, V. Ramani and S. Sankarasubramanian, *ChemSusChem*, 2025, **18**, e202401205.
30 S. Yousuf, M. M. Mridha and R. Magri, *Mater. Adv.*, 2024, **5**, 2069–2087.
31 M. Bianchini, M. Roca-Ayats, P. Hartmann, T. Brezesinski and J. Janek, *Angew. Chem., Int. Ed.*, 2019, **58**, 10434–10458.
32 H. K. Amusa, T. Lemaoui, G. Almustafa, A. S. Darwish, F. Banat, H. A. Arafat and I. M. AlNashef, *Chem. Eng. J.*, 2024, **499**, 156114.
33 R. Liu, J. Li, X. Liu, X. Yin and Y. Yang, *Sep. Purif. Technol.*, 2025, **354**, 128934.
34 R. Morina, E. Carena, N. Pianta, E. Perona, I. Ostroman, P. Mustarelli and C. Ferrara, *J Environ. Manage.*, 2024, **370**, 122827.
35 J. R. Brusas and E. M. B. Dela Pena, *J. Electrochem. Sci. Technol.*, 2021, **12**, 387–397.
36 I. M. Pateli, D. Thompson, S. S. M. Alabdullah, A. P. Abbott, G. R. T. Jenkin and J. M. Hartley, *Green Chem.*, 2020, **22**, 5476–5486.
37 P. G. Schiavi, P. Altimari, E. Sturabotti, A. Giacomo Marrani, G. Simonetti and F. Pagnanelli, *ChemSusChem*, 2022, **15**, e202200966.
38 D. Panias, M. Taxiarchou, I. Paspaliaris and A. Kontopoulos, *Hydrometallurgy*, 1996, **42**, 257–265.
39 L. Sun and K. Qiu, *Waste Manage.*, 2012, **32**, 1575–1582.
40 X. Xiao, B. W. Hoogendoorn, Y. Ma, S. Ashoka Sahadevan, J. M. Gardner, K. Forsberg and R. T. Olsson, *Green Chem.*, 2021, **23**, 8519–8532.
41 C. Padwal, H. D. Pham, S. Jadhav, T. T. Do, J. Nerkar, L. T. M. Hoang, A. Kumar Nanjundan, S. G. Mundree and D. P. Dubal, *Adv. Energy Sustainability Res.*, 2022, **3**, 2100133.
42 X. Chen, B. Fan, L. Xu, T. Zhou and J. Kong, *J. Cleaner Prod.*, 2016, **112**, 3562–3570.
43 M. Chirea, A. Freitas, B. S. Vasile, C. Ghitulica, C. M. Pereira and F. Silva, *Langmuir*, 2011, **27**, 3906–3913.
44 M. H. Shafie, R. Yusof and C.-Y. Gan, *J. Mol. Liq.*, 2019, **288**, 111081.
45 C.-D. Gu and J.-P. Tu, *RSC Adv.*, 2011, **1**, 1220.
46 J. A. Juma, H. K. Ismail, W. O. Karim and S. J. Salih, *Arabian J. Chem.*, 2021, **14**, 102966.
47 W. Liu, A. Migdisov and A. Williams-Jones, *Geochim. Cosmochim. Acta*, 2012, **94**, 276–290.
48 M. Malik, K. H. Chan and G. Azimi, *RSC Adv.*, 2021, **11**, 28014–28028.
49 A. P. Abbott, A. Ballantyne, R. C. Harris, J. A. Juma, K. S. Ryder and G. Forrest, *Electrochim. Acta*, 2015, **176**, 718–726.
50 M. Clotilde Apua and M. S. Madiba, *J. Taiwan Inst. Chem. Eng.*, 2021, **121**, 313–320.
51 Q. Meng, Y. Zhang, P. Dong and F. Liang, *J. Ind. Eng. Chem.*, 2018, **61**, 133–141.
52 H. H. Wang, G. Q. Li, D. Zhao, J. H. Ma and J. Yang, *Hydrometallurgy*, 2017, **171**, 61–68.
53 S. Tang, M. Zhang and M. Guo, *ACS Sustainable Chem. Eng.*, 2022, **10**, 975–985.

54 B. Li, Q. Li, Q. Wang, X. Yan, M. Shi and C. Wu, *Phys. Chem. Chem. Phys.*, 2022, **24**, 19029–19051.
55 P. Kalyani and N. Kalaiselvi, *Sci. Technol. Adv. Mater.*, 2005, **6**, 689–703.
56 P. G. Schiavi, P. Altimari, M. Branchi, R. Zanoni, G. Simonetti, M. A. Navarra and F. Pagnanelli, *Chem. Eng. J.*, 2021, **417**, 129249.
57 A. Urcezino, L. dos Santos, P. Casciano, A. Correia and P. de Lima-Neto, *J. Braz. Chem. Soc.*, 2017, **28**, 1193–1203.
58 W. O. Karim, A. P. Abbott, S. Cihangir and K. S. Ryder, *Trans. IMF*, 2018, **96**, 200–205.
59 N. Peeters, K. Janssens, D. de Vos, K. Binnemans and S. Riaño, *Green Chem.*, 2022, **24**, 6685–6695.
60 F. C. Anson, *Anal. Chem.*, 1966, **38**, 54–57.
61 M. G. Trachioti, A. Ch. Lazanas and M. I. Prodromidis, *Microchim. Acta*, 2023, **190**, 251.
62 P. Sebastian, M. I. Giannotti, E. Gómez and J. M. Feliu, *ACS Appl. Energy Mater.*, 2018, **1**, 1016–1028.
63 M. Klein and S. R. Waldvogel, *Angew. Chem., Int. Ed.*, 2022, **61**, e202204140.
64 M. Girgis and E. Ghali, *Can. J. Chem.*, 1989, **67**, 130–136.
65 P. A. Huttunen, J. Mäkinen and A. Vehanen, *Phys. Rev. B:Condens. Matter Mater. Phys.*, 1990, **41**, 8062–8074.
66 A. Jain, S. P. Ong, G. Hautier, W. Chen, W. D. Richards, S. Dacek, S. Cholia, D. Gunter, D. Skinner, G. Ceder and K. A. Persson, *APL Mater.*, 2013, **1**, 011002.
67 X. Chen, R. Meng, J. Jiang, Q. Liang, Q. Yang, C. Tan, X. Sun, S. Zhang and T. Ren, *Phys. Chem. Chem. Phys.*, 2016, **18**, 16302–16309.
68 A. V. Ruban, H. L. Skriver and J. K. Nørskov, *Phys. Rev. B:Condens. Matter Mater. Phys.*, 1999, **59**, 15990–16000.
69 J. K. U. Ling and K. Hadinoto, *Int. J. Mol. Sci.*, 2022, **23**, 3381.
70 Y. Hua, Y. Sun, F. Yan, S. Wang, Z. Xu, B. Zhao and Z. Zhang, *Chem. Eng. J.*, 2022, **436**, 133200.
71 M. K. Tran, M.-T. F. Rodrigues, K. Kato, G. Babu and P. M. Ajayan, *Nat Energy*, 2019, **4**, 339–345.
72 D. Si, B. Xiong, L. Chen and J. Shi, *Chem Catal.*, 2021, **1**, 941–955.
73 J. Li, L. Li, X. Ma, X. Han, C. Xing, X. Qi, R. He, J. Arbiol, H. Pan, J. Zhao, J. Deng, Y. Zhang, Y. Yang and A. Cabot, *Adv. Sci.*, 2023, **10**, 2300841.
74 X. Yang, Y. Zhang, Q. Meng, P. Dong, P. Ning and Q. Li, *RSC Adv.*, 2021, **11**, 268–277.
75 Q. Lu, L. Chen, X. Li, Y. Chao, J. Sun, H. Ji and W. Zhu, *ACS Sustainable Chem. Eng.*, 2021, **9**, 13851–13861.
76 A. J. Bard, R. Parsons, J. Jordan, *Standard Potentials in Aqueous Solution*, Routledge, 2017.